Palestine Technical University Research Journal, 2024, 12(2), 54-79

Adaptive Model Predictive Control of Yaw Rate and Lateral Acceleration for an Active Steering Vehicle Based on Tire Stiffness Estimation

نموذج تكيفي للتحكم التنبئي في معدل الانعراج والتسارع الجانبي لمركبة توجيه نشطة بناءً على تقدير صلابة الإطارات

Mohammed Assi[1], Mohammed Amer[2*], Başar Özkan[3]

محمد عاصي [1]، محمد عامر [2*]، بشار أوزكان[3]

[1] Department of Automotive Engineering, Palestine Technical University – Kadoorie, Tulkarm, Palestine, [2] Department of Mechanical Engineering, Palestine Technical University – Kadoorie, Tulkarm, Palestine, [3] Istanbul Okan University, Istanbul, Turkey

[1] قسم هندسة السيارات، جامعة فلسطين التقنية - خضوري، طولكرم، فلسطين، [2] قسم الهندسة الميكانيكية، جامعة فلسطين التقنية - خضوري، طولكرم، فلسطين، [3] جامعة اسطنبول أوكان، اسطنبول، تركيا

Received: 11/10/2023 **Accepted: 28/03/2024** **Published: 31/08/2024**

Abstract: Dynamic systems for vehicles are commonly established based on physical rules that are simplified and are not accurately reflective of their dynamic characteristics under certain operating conditions, affecting their accuracy and safety. This paper presents an adaptive model predictive controller (AMPC) with an estimator that controls the yaw rate and lateral acceleration of a realistic ground vehicle. A number of vehicle parameters are estimated using different advanced estimators, of which recursive least squares is one that is widely used. AMPCs and estimators are used to manage the driving process in order for vehicles to remain stable and controllable. In this research, experiments were conducted on a realistic vehicle based on a nonlinear brush tire model. In this estimator, lateral force measurements are analyzed to estimate the tire cornering stiffnesses that are used in the AMPC from a linear bicycle model (lateral force model), where each parameter describes the nonlinearity of the vehicle model. The results demonstrate that the controlled vehicle's performance is improved by combining a recursive least squares estimator with an AMPC in the simulation process. As tire stiffness estimates become more accurate, AMPC performance improves. Yet, AMPC controllers are described in terms of a table of design parameters. As different steering inputs are applied to different vehicles, the yaw rate and lateral acceleration are varied, while tire stiffness is determined. According to the results of this paper, the proposed method for estimating tire-cornering stiffness exhibits high estimation accuracy, robustness, computational efficiency, stability, comfort, and accuracy and reliability under a variety of steering input maneuvers using an AMPC controller.

Keywords: Adaptive model predictive control; Brush tire model; Vehicle stability control; Tire cornering stiffness; least regression square estimation.

* **Corresponding Author E-mail: mohammad.amer@ptuk.edu.ps**

المستخلص: يتم عادةً إنشاء الأنظمة الديناميكية للمركبات بناءً على قواعد فيزيائية مبسطة ولا تعكس بدقة خصائصها الديناميكية في ظل ظروف تشغيل معينة، مما يؤثر على دقتها وسلامتها. تقدم هذه الورقة وحدة تحكم تنبؤية للنموذج التكيفي مع مقدر يتحكم في معدل الانحراف والتسارع الجانبي لمركبة أرضية واقعية. يتم تقدير عدد من معلمات المركبات باستخدام مقدرات متقدمة مختلفة، منها المربعات الصغرى العودية التي تستخدم على نطاق واسع. تُستخدم وحدات التحكم والمقدرات التنبؤية للنموذج التكيفي لإدارة عملية القيادة حتى تظل المركبات مستقرة ويمكن التحكم فيها. أجريت في هذا البحث تجارب على مركبة واقعية تعتمد على نموذج إطار فرشاة غير خطي. في هذا المقدر، يتم تحليل قياسات القوة الجانبية لتقدير صلابة الإطارات عند المنعطفات المستخدمة في وحدة التحكم التنبئية للنموذج التكيفي من نموذج دراجة خطية (نموذج القوة الجانبية)، حيث تصف كل معلمة اللاخطية لنموذج السيارة. توضح النتائج أن أداء السيارة المتحكم فيها قد تم تحسينه من خلال الجمع بين مقدر المربعات الصغرى التكراري ووحدة التحكم التنبؤية للنموذج التكيفي في عملية المحاكاة. عندما تصبح تقديرات صلابة الإطارات أكثر دقة، يتحسن أداء وحدة التحكم التنبؤية للنموذج التكيفي. ومع ذلك، يتم وصف وحدات التحكم التنبؤية النموذجية التكيفية من حيث جدول معلمات التصميم. نظرًا لتطبيق مدخلات توجيه مختلفة على مركبات مختلفة، يتنوع معدل الانعراج والتسارع الجانبي، بينما يتم تحديد صلابة الإطارات. وفقا لنتائج هذا البحث، فإن الطريقة المقترحة لتقدير صلابة الإطارات عند المنعطفات تظهر دقة تقدير عالية، ومتانة، وكفاءة حسابية، وثبات، وراحة، ودقة وموثوقية في ظل مجموعة متنوعة من مناورات إدخال التوجيه باستخدام وحدة تحكم تنبؤية للنموذج التكيفي.

الكلمات المفتاحية: التحكم التنبئي للنموذج التكيفي؛ نموذج إطار الفرشاة؛ التحكم في ثبات السيارة؛ صلابة الإطارات عند المنعطفات؛ أقل تقدير لمربع الانحدار.

1 INTRODUCTION

Engineers in the field of automotive mechatronics use modern technologies in order to enhance vehicle safety. Numerous industrial sectors, ranging from small to large companies, are also engaged in the development of vehicle dynamics and control. In recent years, advanced driver assistance systems (ADAS), such as electronic stability control (ESC) and autonomous emergency braking (AEB), have led to improvements in traffic safety and driving comfort in intelligent vehicles (Wang et al., 2022). Additionally, the development of advanced control systems for various types of vehicles under different conditions has increased in recent decades (Chen et al., 2023; Yahagi & Suzuki, 2023). Consequently, modern vehicle technologies may reduce traffic congestion, energy consumption, pollution, and driving errors as well as prevent accidents (Mietzner et al., 2009). Every day, approximately 3700 people are killed in road traffic collisions around the world (Blagojevic & Ivanis, 2012). The average number of passengers in a vehicle in 2018 was approximately 1.5 million, and it is imperative that the safety of these passengers be ensured (Global Road Safety, 2023). As a potential solution to these problems, autonomous vehicles have attracted considerable interest (Yurtsever et al., 2020). Nevertheless, systems for estimating and controlling friction are extremely important in many applications, such as braking, autonomous vehicles, racing, and stability control. The estimation of tire-road friction coefficients has always been a hot topic in vehicle control. Additionally, this is a significant consideration when it comes to electric vehicles (EVs) with four-wheel independent steering and driving (Eskandarian et al., 2019). In the context of autonomous driving, intelligent tire systems present promising solutions for achieving precise vehicle state estimations, localization, stability, and motion control (Davis & Boundy, 2021). By maximizing tire

saturation in high sideslip drifting maneuvers, autonomous vehicles are capable of substantially improving their handling capabilities.

A large number of singular motion control methods have been developed in conventional drifting controllers, but these methods are not suitable for general driving needs (Zhang et al., 2023). There are many traditional controllers available in the conventional method, such as the PI controller, which are incapable of realizing the desired yaw-rate response due to the fact that the yaw-rate characteristics of the vehicle change with vehicle velocity (Xu et al., 2023). As a result of the characteristics of ASV's operation, autonomous driving and intelligent control are of utmost importance. Throughout the intelligent control process, the tire-road friction coefficient plays a very important role in determining the extreme tire force directly. A suitable control method must therefore be selected that is compatible with the used vehicle and parameters in order to ensure the professional control of the vehicle. In the field of vehicle dynamics, model predictive controllers are widely used. They are considered to be the most appropriate control technique for handling vehicle dynamics (Hajiloo et al., 2020). As well as being used to resolve conflicts between collision avoidance, vehicle stability, and path tracking control objectives, it has also been utilized to address conflicts between them (Gao et al., 2021). One example is the use of a nonlinear model predictive direct yaw moment control alongside trailer sway mitigation (De Bernardis et al., 2023). Moreover, a regenerative braking control for distributed drive EVs has been developed based on least square estimation of the slope of the road and the mass of the vehicle (Chen et al., 2023). As part of conditional automation and partially automated driving, adaptive cruise control systems have been introduced (Shakouri & Ordys, 2014). Automated driving includes a variety of levels, including automated driving decisions (Nilsson et al., 2016), trajectory planning (Li et al., 2015), and path tracking control (Wang et al., 2016).

Vehicles are typically equipped with advanced control systems to enhance fuel economy, emissions, passenger comfort, stability, and safety. Modern vehicle control systems require accurate knowledge of a vehicle's side slip and yaw rate (Daily & Bevly, 2004). A linear model of a vehicle is updated using estimated values of cornering stiffness or side slip angle. It has recently been demonstrated that a GPS attitude system with two antennas is capable of directly measuring sideslip because it provides both a velocity vector and a true heading (Nishio et al., 2001; Zhang et al., 2016). Over the past few decades, extensive research has been conducted on the development of tire models. Therefore, different tire models have been proposed and applied to the design of estimators and controllers, such as the Magic Formula, the Dug-off model, Pacejka's tire model, and the Brush model. For the purpose of simulating a controller for a vehicle, a nonlinear model of the vehicle is used in this paper where the nonlinear vehicle model consists of four nonlinear tires. Furthermore, the model incorporates the transfer of weight between tires. Yet, adaptive model predictive control is employed to control the system. In this controller, linear tire models are used in conjunction with a bicycle model. For the purpose of estimating the stiffness of linear tires, measurements are made of a "real" nonlinear vehicle. By means of model reference control, adaptive model predictive controllers are provided with reference yaw rates. Finally, for the purpose of producing the optimal yaw rate response for the steering input of the driver, an ideal bicycle model vehicle is used as a reference.

Section 2 describes the linear bicycle model, which is used as an ideal reference to generate reference yaw rate and lateral acceleration. In Section 3, a nonlinear four-wheel car model is presented with both longitudinal and lateral directions, controlling the vehicle as if it were a "real" vehicle by means of suitable nonlinear tire formulas. Real vehicles are described by the Ackerman condition. To ensure a more realistic model, a weight transfer model is also taken into account for each tire. Additionally, aerodynamic effects are also applied to the longitudinal direction of the vehicle. The fourth section explains the estimator and illustrates how it can be used to estimate tire stiffness using simulations. In Section 5, an AMPC with an estimator is presented to control the vehicle's yaw rate and acceleration by default. In Sections 5 and 6, several simulations are presented to demonstrate how steering input variance affects the system's cornering stiffness and outputs. The simulations are conducted using realistic values for the parameters of the vehicles using the MATLAB simulation program.

2 REFERENCE MODEL

In this section, the linear lateral dynamics tire force bicycle model with two degrees of freedom will be introduced, which will provide an ideal yaw rate as a reference for the AMPC to be used in the subsequent section. The states of the system are represented by the yaw rate r and the lateral velocity v_y. In view of the fact that it utilizes a lateral dynamic model, the longitudinal velocity v_x remains constant. A schematic diagram of the bicycle model is shown in Figure 1. The lateral dynamic equations of motion for a bicycle model with a mass m are given below:

$$m(\dot{v}_y + r v_x) = F_{yf} + F_{yr} \quad (1)$$

$$I_z \dot{r} = -l_r F_{yf} + l_r F_{yr} \quad (2)$$

Where F_{yf} and F_{yr} are lateral rear force and lateral front force respectively. I_z is mass moment of inertia of the vehicle. At high speeds, steering produces small slip angles to maintain linear forces as in the following equations:

$$F_{yf} = C_f \alpha_f \quad (3)$$

$$F_{yr} = C_r \alpha_r \quad (4)$$

Where C_f and C_r are front and rear cornering stiffness coefficients respectively. Something to notice is that the cornering stiffness coefficients as well as the yaw moment of inertia cannot be accurately identified in practice so they can be estimated (Nishio et al., 2001). Small front and rear lateral slip angles (α_f and α_r) are calculated as in equations (5) and (6):

$$\alpha_r = \frac{v_y - r l_r}{v_x} \quad (5)$$

$$\alpha_f = \frac{v_y + r l_f}{v_x} - \delta \quad (6)$$

Where l_f is the distance from front axle to the center of gravity and l_r is the distance from rear axle to the center of the gravity, δ is the steering input. Substituting equations (3), (4) into (1), (2):

$$m(\dot{v}_y + r v_x) = -C_r \alpha_r - C_f \alpha_f \quad (7)$$

$$I_z \dot{r} = -l_r C \alpha_r + l_f C_f \alpha_f \quad (8)$$

Combining equations (5), (6) to (7), (8) obtains the state equations as in the following:

$$\dot{v}_y = \frac{-(C_r + C_f)}{m v_x} v_y - \frac{-(C_r l_r + l_f C_f)}{m v_x} r - \frac{C_f}{m}\delta \quad (9)$$

$$\dot{r} = -\frac{(l_r C_r - l_f C_f)}{I_z v_x} v_y - \frac{(l_r{}^2 C_r - l_f{}^2 C_f)}{I_z v_x} v_y + \frac{l_f C_f}{I_z}\delta \quad (10)$$

The previous two equations can be easily presented by state a space model matrix form as shown in equations (11) and (12) below:

$$\dot{x} = Ax + Bu \quad (11)$$

$$y = Cx \quad (12)$$

From equations (9) and (10), the matrices for state space presentation is shown in equations (13) and (14):

$$\begin{bmatrix} \dot{v}_y \\ \dot{r} \end{bmatrix} = \begin{bmatrix} \frac{-(c_f + c_r)}{m v_x} & \frac{-(l_f c_f - l_r c_r)}{m v_x} - v_x \\ \frac{-(l_f c_f - l_r c_r)}{m I_z} & \frac{-(l_f{}^2 C_f - l_r{}^2 C_r)}{m I_z} \end{bmatrix} \begin{bmatrix} v_y \\ r \end{bmatrix} + \begin{bmatrix} \frac{C_f}{m} \\ \frac{-a C_f}{I_z} \end{bmatrix} \delta \quad (13)$$

$$y = C \begin{bmatrix} v_y \\ r \end{bmatrix} \quad (14)$$

Where C is a 2×2 identity matrix to demonstrate that both states of lateral velocity and yaw rate are available as well.

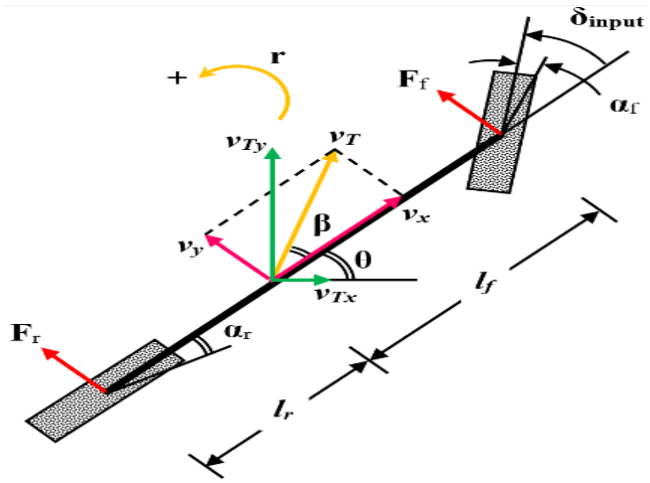

Figure (1). Schematic diagram of bicycle model.

3 FOUR TIRES CAR MODEL

In this section, a proposed model of a car will be derived and modeled. Figure 2 illustrates the dynamic four-tire model.

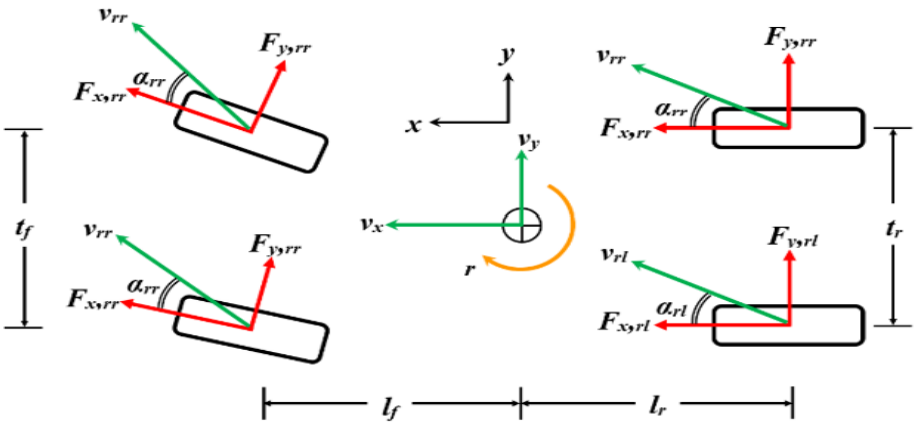

Figure (2). Four tires car model.

3.1 Steering Commands

Since a four-wheeled car model includes both right and left steering, there will be inner and outer steering wheels as can be seen in Figure 3. If a vehicle turns left, for example, the right front wheel becomes the inner wheel and rotates more than the left front wheel, which is the outer wheel. This can, however, be accomplished easily by using the car's differential. Geometries should include inner and outer steering angles that are calculated and updated according to the input steering from the user or controller.

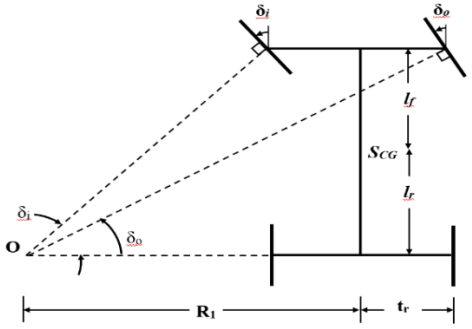

Figure (3). Ackermann condition for steering system.

The following equations represent the symbols in Ackermann condition for steering systems:

$$R_1 = (l_f + l_r)\,cot(\delta) \tag{15}$$

$$tan(\delta_i) = \frac{l_f + l_r}{R_1 - \frac{t_r}{2}} \tag{16}$$

$$\delta_i = tan^{-1}\left(\frac{l_f + l_r}{(l_f + l_r)\,cot(\delta) + \frac{t_r}{2}}\right) \tag{17}$$

$$\tan(\delta_o) = \frac{l_f + l_r}{R_1 + \frac{t_r}{2}} \tag{18}$$

$$\delta_o = \tan^{-1}\left(\frac{l_f + l_r}{(l_f + l_r)\,\cot(\delta) + \frac{t_r}{2}}\right) \tag{19}$$

Inner and outer wheels are defined during turns depending on the steering angle of the user or controller as in equations (20) and (21):

$$\delta_{fr} = \begin{cases} \delta_i, & \delta_{input} < 0 \\ \delta_o, & \delta_{input} \geq 0 \end{cases} \quad (20)$$

$$\delta_{fl} = \begin{cases} \delta_o, & \delta_{input} < 0 \\ \delta_i, & \delta_{input} \geq 0 \end{cases} \quad (21)$$

4 FOUR TIRES VEHICLE MODEL

In this section, a proposed vehicle model will be derived and modeled. Figure 2 shows the dynamic four tire model.

4.1 Slip angle calculations

The four-tire model uses both longitudinal and lateral forces which means it maintains variable longitudinal velocity. Slip angles are calculated in equations (22), (23), (24) and (25):

$$\alpha_{fr} = \frac{v_x + rl_f}{v_x - r\,\frac{t_f}{2}} - \delta_{fr} \quad (22)$$

$$\alpha_{fl} = \frac{v_x + rl_f}{v_x + r\,\frac{t_f}{2}} - \delta_{fl} \quad (23)$$

$$\alpha_{rr} = \frac{v_x - rl_r}{v_x - r\,\frac{t_r}{2}} \quad (24)$$

$$\alpha_{rl} = \frac{v_x - rl_r}{v_x + r\,\frac{t_r}{2}} \quad (25)$$

4.2 Force and moment equations

The dynamic equations for the car model are expressed as three degrees of freedom (3 DOF). The lateral, longitudinal and yaw rate of the four-tire vehicle model is obtained from equations (26), (27) and (28):

$$m(\dot{v}_y + v_x r) = F_{y,fr} + Fy,_{fl} + F_{y,rr} + F_{y,rl} \quad (26)$$

$$m(\dot{v}_x + v_y r) = F_{x,fr} + F_{x,fl} + F_{x,rr} + F_{x,rl} - F_d \quad (27)$$

$$I_z\dot{r} = l_f F_{y,fr} + l_f F_{y,fl} - l_r F_{y,rr} - l_r F_{y,rl} - \frac{t_f}{2}F_{x,fr} + \frac{t_f}{2}F_{x,fl} - \frac{t_f}{2}F_{x,rr} + \frac{t_f}{2}F_{x,rl} \quad (28)$$

where F_d is aerodynamic drag force. The aerodynamic formula is as in equation (29):

$$F_d = \frac{1}{2}\rho A c_d {v_x}^2 \quad (29)$$

where ρ is the air density 1.225 kg/m^3, A is the front area m^2 and c_d is the drag coefficient and it is equal to 0.12.

4.3 Weight transfer model

It is imperative to take into account the change of the normal forces on the vehicle tires as the vehicles weight transfers between them in order to calculate accurate friction usage during high acceleration as the vehicle operates close to the limits of handling. Assuming that the vehicle acts as a rigid body, the normal forces on the front and rear axles can be calculated by taking into account the longitudinal weight transfer due to ax as well as follow:

$$F_{zf} = m\left(\frac{l_r g - h_{CG}\, a_x}{L}\right) \quad (30)$$

$$F_{zr} = m\left(\frac{l_f g + h_{CG}\, a_x}{L}\right) \quad (31)$$

where g is the gravitational acceleration, h_{CG} is the vertical distance from the center of gravity of the vehicle to the ground and L is the wheelbase, which is the sum of l_f and l_r.

The amount of lateral weight transfer on each axle is calculated as follows:

$$\Delta F_{zf} = \frac{h_f(F_{yfl} + F_{yfr})}{d} \quad (32)$$

$$\Delta F_{zr} = \frac{h_r(F_{yfr} + F_{yrr})}{d} \quad (33)$$

where h_f and $h_r$are the heights of the front and rear roll centers from the ground, respectively. The normal forces are used as inputs to the system during tire-force calculation to present the effect on the outputs. The normal force on each wheel due to weight transfer can be calculated as in the series of equations (34), (35), (36) and (37):

$$F_{zfr} = \frac{F_{zf}}{2} + \Delta F_{zf} \tag{34}$$

$$F_{zfl} = \frac{F_{zf}}{2} - \Delta F_{zf} \tag{35}$$

$$F_{zrr} = \frac{F_{zr}}{2} + \Delta F_{zr} \tag{36}$$

$$F_{zfl} = \frac{F_{zr}}{2} - \Delta F_{zr} \tag{37}$$

4.4 Couple brush tire model

This paper uses a modified version of Pacejka's combined slip brush tire model (Pacejka, 2005). For a given tire slip angle α and a longitudinal slip k as in equation (38), the weighted vector norm of the theoretical slip quantities f is defined as follows:

$$k = \frac{\omega r_e - v_x}{v_x} \tag{38}$$

$$f = \sqrt{(C_x \sigma_x)^2 + \left(C_\alpha \sigma_y\right)^2} \tag{39}$$

where σ_x and σ_y are the theoretical longitudinal and lateral slips respectively as in equations (40) and (41).

$$\sigma_x = \frac{k}{1+k} \tag{40}$$

$$\sigma_y = \frac{\tan \alpha}{1+k} \tag{41}$$

and C_x and C_α are the longitudinal and lateral tire stiffnesses, respectively. The magnitude of the total force on the tire F is given as follows:

$$F = \begin{cases} f - \frac{1}{3\mu F_z} f^2 + \frac{1}{27\mu^2 {F_z}^2} f^3 & , f \le 3\mu F_z \\ \mu F_z & , f > 3\mu F_z \end{cases} \tag{42}$$

The total force F is projected into longitudinal and lateral components F_x and F_y according to the ratio of the slip quantities.

$$(F_{tx}, F_{ty}) = \left(\frac{C_x \sigma_x}{f} F, \frac{-C_\alpha \sigma_y}{f} F\right) \quad (43)$$

5 FRICTION ESTIMATION

For friction estimation purposes it is assumed that tire forces and slip angles are measured from a "real" vehicle. It is assumed that tire force sensors are available. Tire force sensors that are economical feasible are currently under development (Hayward et al., 1999). Slip angles can also be measured using GPS signals (Cohen et al., 1994; Acosta et al., 2019). Figure 4 shows the estimator process diagram.

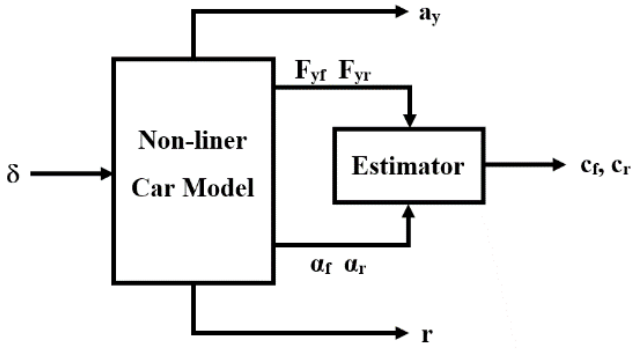

Figure (4). Estimator process diagram.

The cornering stiffness coefficients are estimated based on the linear equation as follows:

$$F(t) = C(t)\, \alpha(t) \quad (44)$$

This paper uses recursive least square estimation using the forgetting factor method which can be explained in the following series of equations (45) to (48):

$$\hat{C}(t) = \hat{C}(t-1) + K(t)(F(t) - \hat{F}(t)) \quad (45)$$

$C(t)$ is the cornering stiffness estimated at time t. $F(t)$ is the observed lateral force at time t, and $\hat{F}(t)$ is the prediction of $F(t)$ based on observations up to time $t-1$. The gain, $K(t)$ in (44), determines how much the current prediction error of lateral force $F(t) - \hat{F}(t)$ affects the update of the estimated C.

$$K(t) = Q(t)\, \alpha(t) \quad (46)$$

where $\alpha(t)$ is the regression computed passed on previous values of measured lateral force and stiffness. $Q(t)$ can be obtained by minimizing (46) at time t.

$$Q(t) = \frac{P(t-1)}{\lambda + \alpha(t)^T P(t-1)\, \alpha(t)} \tag{47}$$

Using equation (48), the software computes a positive-definite matrix where the residuals (difference between the estimated and measured outputs) are white noise.

$$P(t) = \frac{1}{\lambda}\left(P(t-1) - \frac{P(t-1)\, \alpha(t)\, \alpha(t)^T P(t-1)}{\lambda + \alpha(t)^T P(t-1)\, \alpha(t)}\right) \tag{48}$$

Estimated cornering stiffness depends on the car's steering input variance. Figure 5. shows how estimated stiffness, lateral acceleration and yaw rate are affected by random step steering input size. Steering inputs 1, 2 and 3 have variances of 3, 5 and 7 degrees, respectively. The car parameters used for simulation are listed in Table 1.

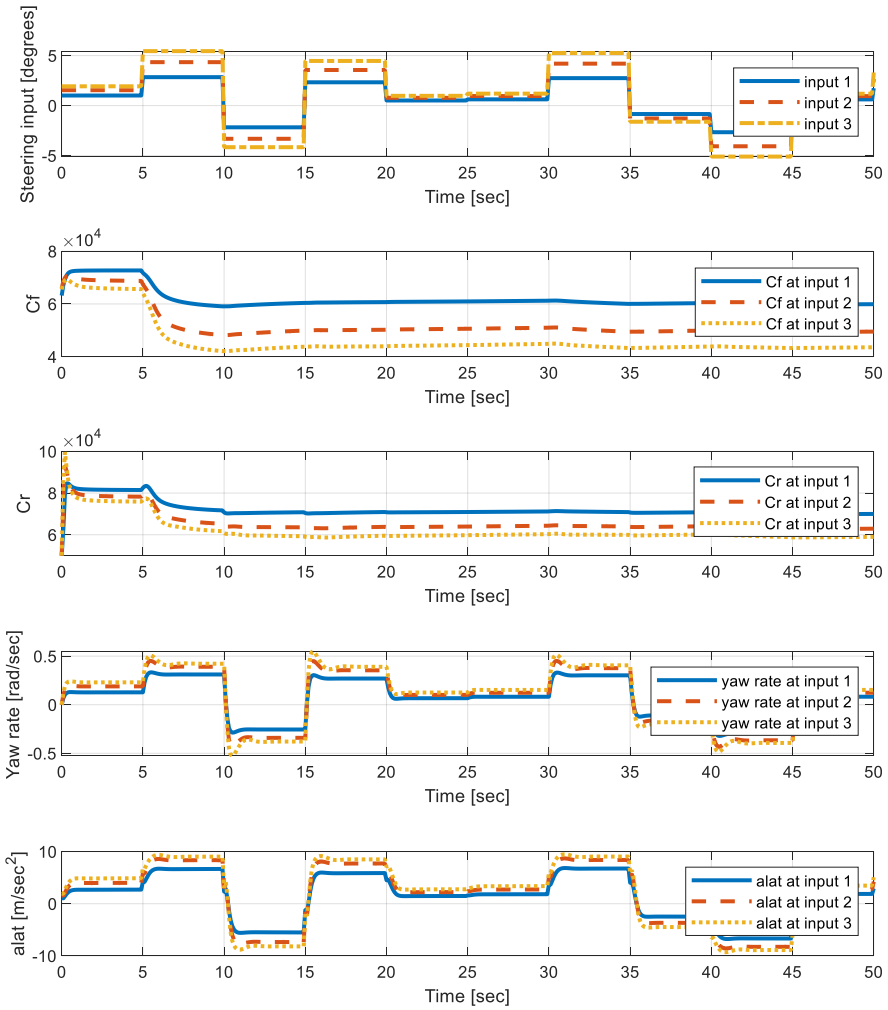

Figure (5). Cornering stiffness estimates for different steering input sizes.

Table 1. Real car parameters

Parameter	Symbol	Value	Unit
Vehicle mass	m	1200	Kg
Yaw moment of inertia	I_z	1500	kg-m^2
Front axle-CG distance	l_f	1	M
Rear axle-CG distance	l_r	1.2	M
Left-right wheels distance	t_r, t_f	1.2	M
ground to CG distance	h_{CG}	0.9	M
Wheel axles to CG distance	h_f, h_r	0.3	M
Car width	t	1.2	M
Wheel base rim radius	r_e	0.3	M
Front area	A	2	m^2
Drag coefficient	c_d	0.12	----
Longitudinal	C_x	50000	N/rad
Lateral	C_α	50000	N/rad

6 MPC CONTROLLER DESIGN

MPC controller deals with a feedback algorithm that optimizes each time step to get the optimal solution. Figure 6 shows a schematic diagram of MPC controller.

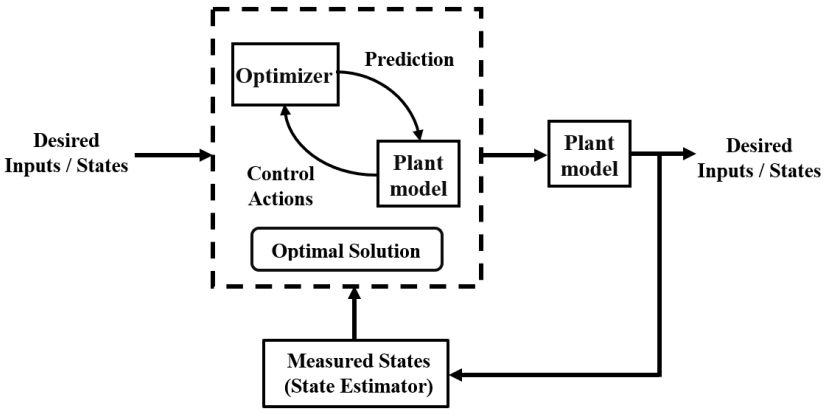

Figure (6). Schematic diagram of MPC controller

The constrained optimization problem can be minimized using the following quadratic programming (QP) method as in equation (49):

$$X^T Hx - g^T x;\ Ex < b \tag{49}$$

where $x = (k)$; H means symmetric matrix, g represents the gradient vector. E and b are the constraint matrices used in the QP. The first element of the optimal sequence $\Delta u(k)$ is to be selected as the solution of the control system.

$$\Delta u(k) = [1,0,\dots,0] \cdot \Delta u(k);\ u(k) = \sum_{i=1}^{k} \Delta u(i) \tag{50}$$

In this desert, the input to the real car's model is presented as the steering input (δ_c) which depends on the additional steering input δ_A and the driver steering input δ_d can be presented as in the following equation (51):

$$\delta_c = \delta_A + \delta_d \tag{51}$$

6.1 Adaptive MPC for yaw rate control

Since the plant is assumed to have unknown tire parameters, an AMPC is used based on linearization. This is such that a linear model is computed as operating conditions change. At each time step, the internal plant simulation is updated by the AMPC controller with a linear bicycle model. Here, cornering stiffness and longitudinal velocity are the variables to be updated. In addition, the steering angle from AMPC states and yaw rate. Figure 6 shows a diagram of the AMPC control process based on tire stiffness estimation.

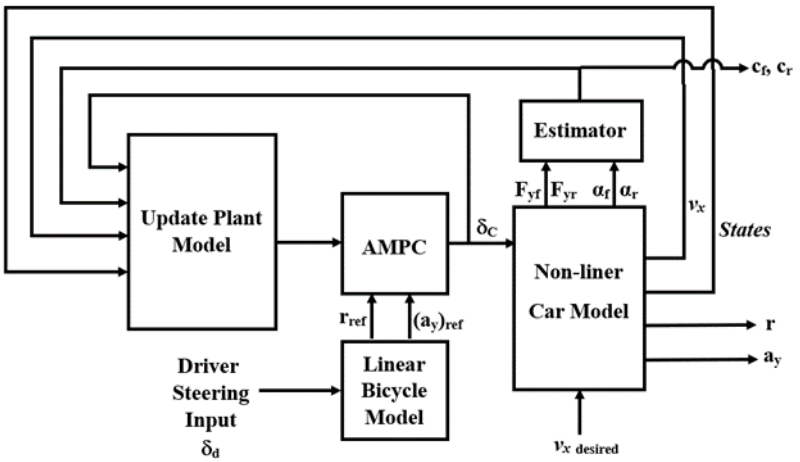

Figure (7). AMPC with friction estimation control process

The plant model used as the basis for adaptive MPC must be an LTI (linear time invariant) discrete-time, state-space model. In adaptive MPC, the nominal operating point should be updated to be consistent with the updated plant model as well. The plant model in terms of deviations from the nominal condition structure is presented in equation (52):

$$x(k+1) = \bar{x} + A(x(k) - \bar{x}) + B(u(k) - \bar{u}) + \overline{\Delta x} \tag{52}$$

$$y(k) = \bar{y} + C(x(k) - \bar{x}) \tag{53}$$

where k is the discrete time step, $\bar{x}$ is the nominal state has the parameters of C_f and C_r to be updated, $\overline{\Delta x}$ is the increment of nominal state, $\bar{u}$ is nominal input matrix and $\bar{y}$ is the nominal output matrix.

$$\overline{\Delta x} = Ax(t) + Bx(t)\text{-}x \tag{54}$$

6.2 Prediction equation design

The plant model in terms of deviations from the nominal condition structure is described as in the equation (52) which a discrete time model for the state space model shown in (11) and (12):

$$x(k+1) = A_c x(k) + B_{cu} u(k) + B_{cd} d(k) \tag{55}$$

$$y(k) = Cx(k) \tag{56}$$

The static error of the system can be eliminated so that the discrete system model as can be written as an incremental type:

$$\Delta x(k+1) = A_c \Delta x(k) + B_{cu} \Delta u(k) + B_{cd} \Delta d(k) \tag{57}$$

$$y(k) = C\Delta x(k) + y(k-1) \tag{58}$$

According to the control horizon M and prediction horizon M, the solution for each discrete time step can be written as in the sequence of equations from (59) to (62). The matric x(k) is to be used as the starting solution of the prediction issue as in (59):

$$\Delta x(k+1|k) = A_c \Delta \hat{x}(k) + B_{cu} u(k) + B_{cd} d(k) \tag{59}$$

$$(k+2|k) = A_c \Delta \hat{x}(k) + B_{cu} u(k+1) + B_{cd} d(k+1) = A_c^2 \Delta \hat{x}(k) + A_c B_{cu} u(k) + B_{cu} d(k+1) + A_c B_{cd} \Delta d(k) \tag{60}$$

$$\Delta x(k+M|k) = A_c^M \Delta \hat{x}(k) + A_c^{M-1} B_{cu} \Delta u(k) + A_c^{M-2} B_{cu} \Delta u(k+1) + \cdots + B_{cu} \Delta u(k+M-1) + A_c^{M-1} B_{cd} \Delta d(k) \tag{61}$$

$$\Delta x(k+P|k) = A_c^P \Delta \hat{x}(k) + A_c^{P-1} B_{cu} \Delta u(k) + A_c^{P-2} B_{cu} \Delta u(k+1) + \cdots + B_{cu} \Delta u(k+P-1) + A_c^{P-1} B_{cd} \Delta d(k) \tag{62}$$

As a result, according to the basis of the predictive states, the predictive outputs at each time step (k) are given as (63):

$$y(k+1|k) = C_c A_c \Delta \hat{x}(k) + C_c B_{cu} u(k) + C_c B_{cd} \Delta d(k) + \hat{y}(k) \tag{63}$$

$$y(k+2|k) = (C_c A_c^2 + C_c A_c)\Delta\hat{x}(k) + (C_c A_c B_{cu} + C_c B_{cu})u(k) + C_c B_{cu}\Delta u(k+1) + (C_c A_c B_{cd} + C_c B_{cd})\Delta d(k) + \hat{y}(k)$$

$$y(k+P|k) = \sum_{i=1}^{P} C_c A_c^i \Delta\hat{x}(k) + \sum_{i=1}^{P} C_c A_c^{i-1} B_{cu}\Delta u(k) + \sum_{i=1}^{P-1} C_c A_c^{i-1} B_{cu}\Delta u(k) + \cdots + \sum_{i=1}^{P-M+1} C_c A_c^{i-1} B_{cu}\Delta u(k+M-1) + \sum_{i=1}^{P} C_c A_c^{i-1} B_{cd}\Delta d(k) + \hat{y}(k) \quad (64)$$

The sequence for the control input rate of change $\Delta U(k)$ and prediction control output $Y(k)$ are defined in (62) and (66) respectively:

$$\Delta U(k) = \begin{bmatrix} \Delta u(k|k) \\ \Delta u(k+1|k) \\ \vdots \\ \Delta u(k+M-1|k) \end{bmatrix}_{M\times 1} \quad (65)$$

$$Y(k+1) = \begin{bmatrix} y(k+1|k) \\ y(k+2|k) \\ \vdots \\ y(k+P|k) \end{bmatrix}_{P\times 1} \quad (66)$$

The value of $\Delta u(k)$ is to be set zero beyond the control horizon. Given that the driver's intention is constantly changing, the reference yaw rate in the prediction horizon is calculated according to the driver's intention. This is to obtain improved control performance. $r_{ref}(k)$ is the reference yaw rate that can be defined in the equations (67) to (69):

$$r_{ref}(k+1) = r_{ref}(k) + \epsilon(r_{ref}(k) - r_{ref}(k-1)) \quad (67)$$

$$r_{ref}(k+2) = r_{ref}(k+1) + \epsilon\left(r_{ref}(k) - r_{ref}(k-1)\right) \quad (68)$$

$$\vdots$$

$$r_{ref}(k+P) = r_{ref}(k+P-1) + \epsilon\left(r_{ref}(k) - r_{ref}(k-1)\right) \quad (69)$$

where ϵ is the weight factor that affects the tracking performance of the real car's model. $a_{y\,ref}(k)$ is the reference yaw rate that can be defined as in equations (70) to (72):

$$a_{y\,ref}(k+1) = a_{y\,ref}(k) + \epsilon(a_{y\,ref}(k) - a_{y\,ref}(k-1)) \quad (70)$$

$$a_{y\,ref}(k+2) = a_{y\,ref}(k+1) + \epsilon\left(a_{y\,ref}(k) - a_{y\,ref}(k-1)\right) \tag{71}$$

$$\vdots$$

$$a_{y\,ref}(k+P) = a_{y\,ref}(k+P-1) + \epsilon\left(a_{y\,ref}(k) - a_{y\,ref}(k-1)\right) \tag{72}$$

The input reference sequence $R(k+1)$ is defined as follows:

$$R(k+1) = \begin{bmatrix} r_{ref}(k+1) & a_{y\,ref}(k+1) \\ r_{ref}(k+2) & a_{y\,ref}(k+2) \\ \vdots & \vdots \\ r_{ref}(k+P) & a_{y\,ref}(k+P) \end{bmatrix}_{P\times 2} \tag{73}$$

6.3 Cost function equations

Performing optimized control problems requires a cost function design for the tracking problem. In this research the main priority is to track the desired rate of yaw rate which defines the first cost function part (J_1). Then the secondary aim is to reduce the rate of change of controlled steering input which defines the second cost function part (J_2). The cost functions are presented as follows:

$$J_1 = |Y(k+1) - R(k+1)|^2_{Q_2} = \sum_{i=1}^{P}\left[r(k+i|k) - r_{ref}(k+i)^2.\,Q_1\right] \tag{74}$$

$$J_2 = |\Delta U(k)|^2_{Q_2} = \sum_{i=1}^{M-1}[\Delta\delta_c(k+i-1|i)^2 Q_2] \tag{75}$$

where Q_1 is the weight factor responsible for tracking performance and Q_2 is responsible for adjusting control inputs. The total cost function for the process of choosing the optimal solution (J) can be written as:

$$J = J_1 + J_2 \tag{76}$$

$$J = \left|\left|Y(k+1) R(k+1)\right|\right|^2_{Q_1} + \left|\left|\Delta U(k)\right|\right|^2_{Q_2} \tag{77}$$

The controller deals with hard constraints which are the limits of steering input (δ_d) and the rate of change of steering inputs ($\Delta\delta_d$). These can be written as follows:

$$-\delta_{c\,min} \leq \delta_c(k+i|k) \leq -\delta_{c\,min} \tag{78}$$

$$-\Delta\delta_{c\,min} \leq \Delta\delta_c(k+i|k) \leq -\delta_{c\,min} \tag{79}$$

where $I = 1, 2, \ldots, M-1$.

The specified design parameters used to control the vehicle using AMPC are tabulated as in Table 2:

Table (2). Real car parameters.

Parameter	Symbol	Value	Unit
MPC prediction horizon	P	20	----
MPC sampling time	T_s	0.001	Sec
MPC control horizon	M	4	----
Minimum steering input constrain	δ_{min}	-π/6	Rad
Maximum steering input constrain	δ_{max}	π/6	Rad
Minimum steering input rate constrain	$\dot{\delta}_{min}$	-15	°/sec
Maximum steering input rate constrain	$\dot{\delta}_{max}$	15	°/sec
Minimum output yaw rate constrains	r_{min}	-0.3	rad/sec
Maximum output yaw rate constrains	r_{max}	0.3	rad/sec
Minimum output lateral acceleration	r_{min}	-4	rad/sec
Maximum output lateral acceleration	r_{max}	4	rad/sec
Weight of inputs	Q_1	0	----
Weight of rate of inputs	Q_2	0.44	----
Weight of outputs		1	----

7 RESULTS AND DISCUSSION

In this section, a comparison of three different vehicles will be conducted through different steering input tests to show the effectiveness of the AMPC controllers and used estimator to observe the yaw rate, lateral acceleration and estimated cornering stiffness and how are they affected. The first test is a sinewave saturated at the absolute value of 3 degrees, the second test is a step steering input with a slope of 10 degrees/sec and saturated at 3 degrees. Both first and second tests are run for 6 seconds. The third test uses a random 3 degrees steering input variance and run for 8 seconds to show the improvement of steering oscillations while estimating correct cornering stiffness of real car model corresponding to the reference inputs from ideal car's model. Each simulation works with 21 m/s.

For the first and second tests, Figures 8 and 13 illustrate the steering inputs for open loop. This is the same for the ideal vehicle and uncontrolled real vehicle, and the steering of controlled vehicles. It is shown that the controlled vehicle with an estimator has a steering input closer to the open loop signal than the controlled vehicle without an estimator. In Figures 9 and 14, the uncontrolled car reached a very high yaw rate, suggesting that the vehicle has become unstable and oversteering. Figures 10 and 15 illustrate the lateral acceleration response. Clearly, the controlled vehicle with cornering stiffness estimation has a

lower yaw rate and lateral acceleration than the vehicle without an estimator, while the uncontrolled vehicle exhibits a high lateral acceleration. For front and rear tires, figures 11 and 16 illustrate the estimated cornering stiffness. Within three seconds, the cornering stiffness reached the correct estimated value, demonstrating the advantages of the controller and estimator. In Figures 12 and 17, the vehicle's XY trajectory is shown. It is demonstrated that the car equipped with the estimator follows ideal XY baths better than other vehicles.

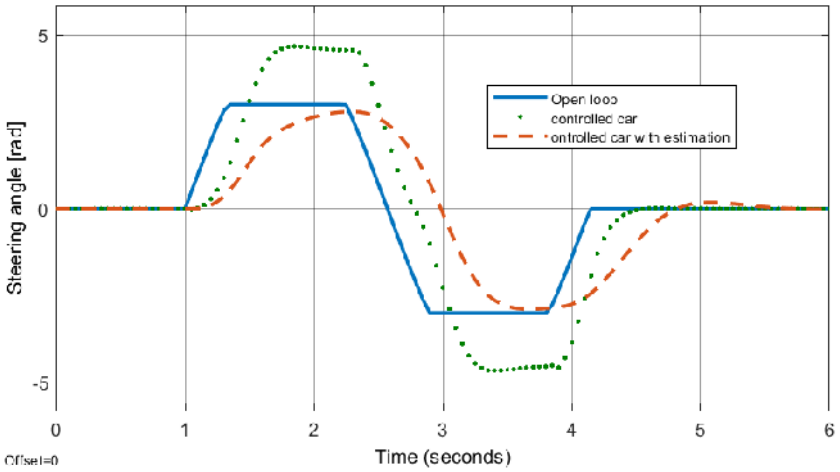

Figure (8). Steering angles in test 1

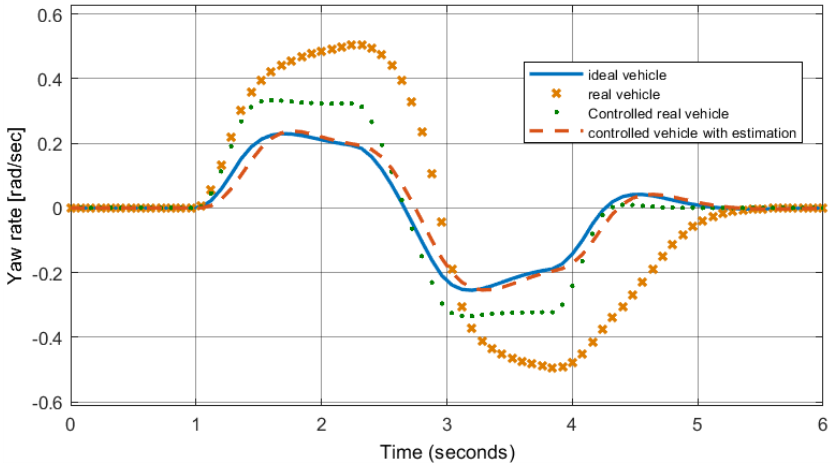

Figure (9). Yaw rate response in test 1

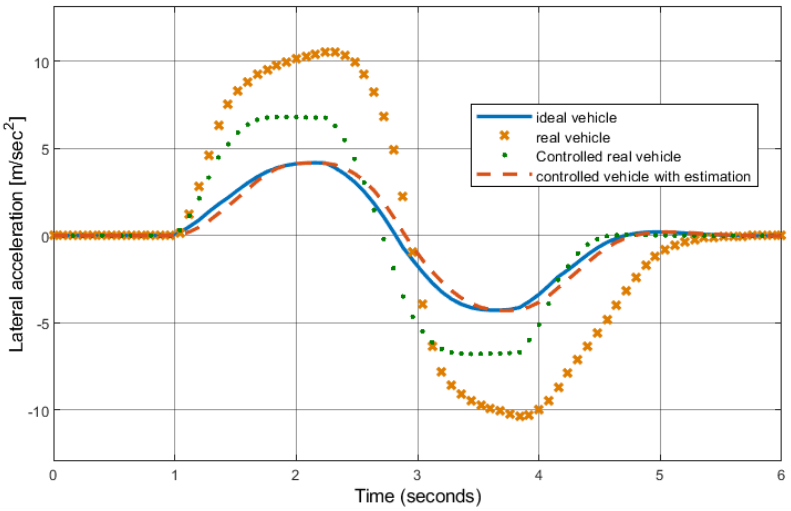

Figure (10). Lateral acceleration response in test 1

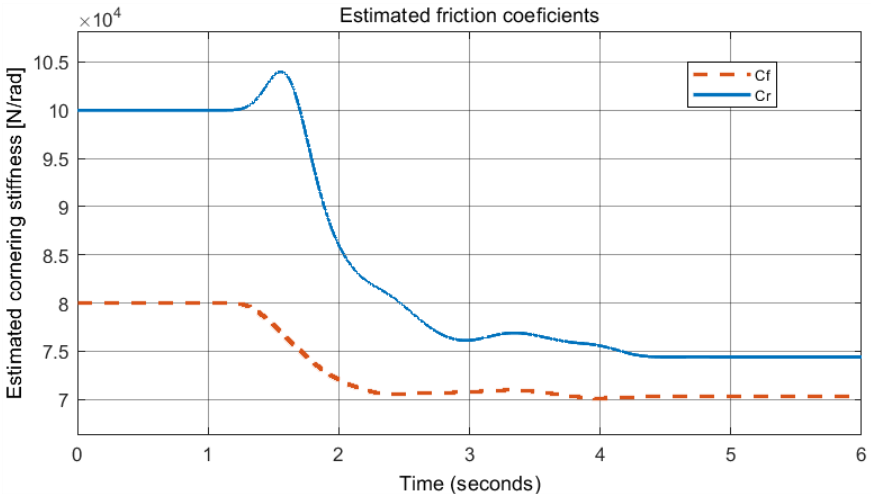

Figure (11).Estimated cornering stiffness in test 1

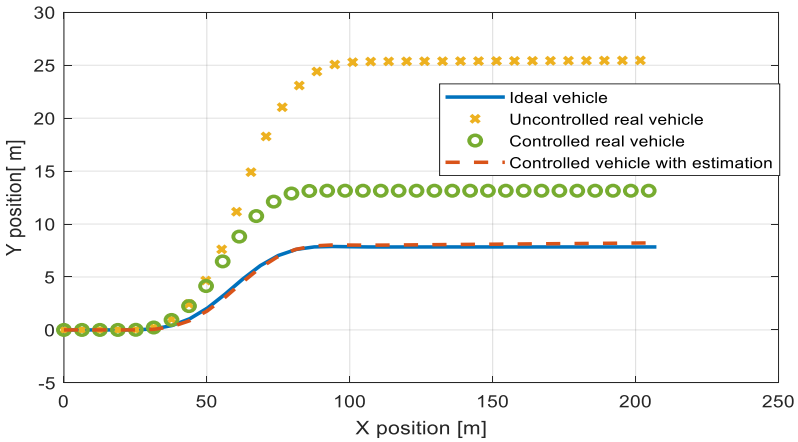

Figure (12). XY trajectory path in test 1

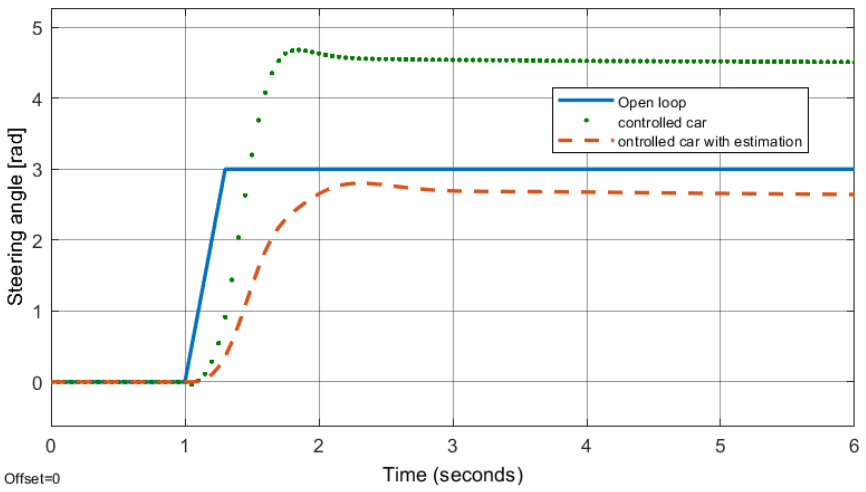

Figure (13) Steering angles in test 2

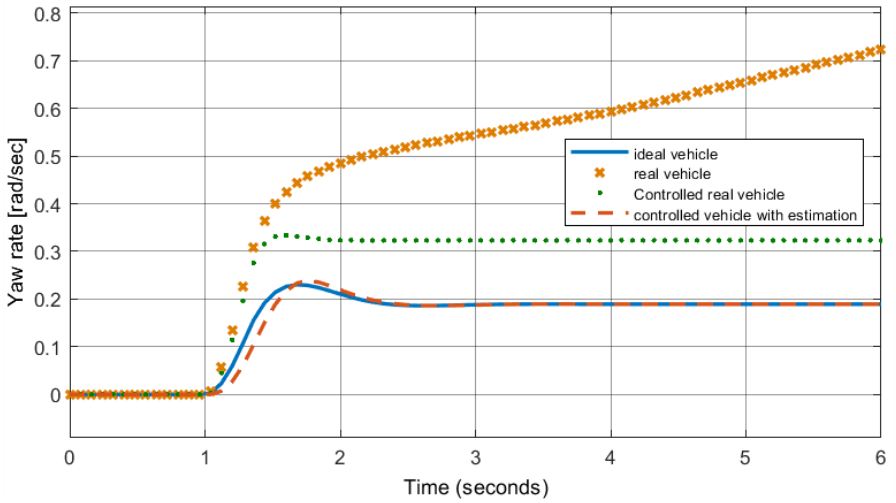

Figure (14) Yaw rate response in test 2

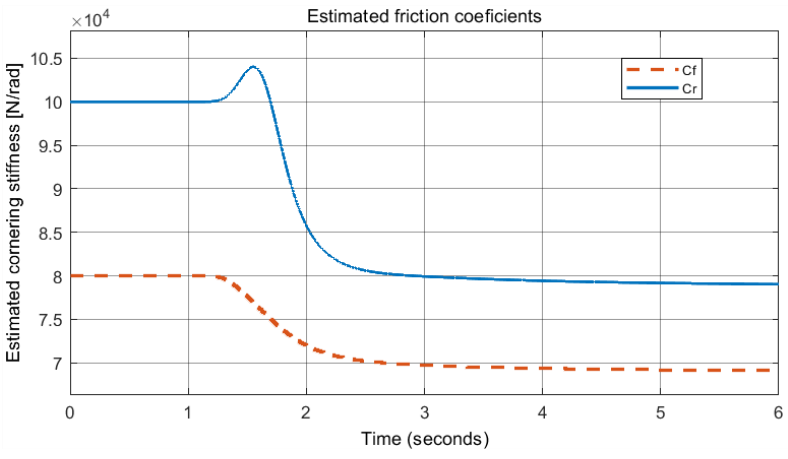

Figure (15).Estimated cornering stiffness in test 2

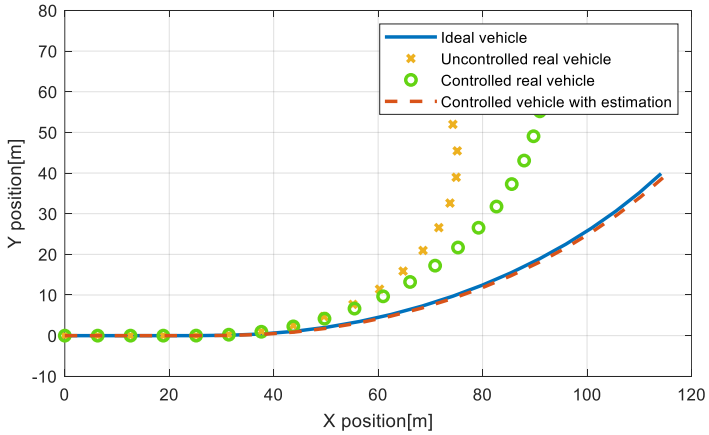

Figure (16). XY trajectory path in test 2

Increasing steering input variance results in reduced cornering stiff nesses, as shown in Figure 6 of Section 5. As a result of high steering inputs, tire forces are expected to saturate. Therefore, at higher slip angles, the tire produces smaller force increases per increase in slip angle, which results in lower tire stiffness.

In Figure 18, the steering angles from the open loop and the AMPC controller are shown, showing that the AMPC steering output oscillates during the first three seconds of the simulation. Conversely, the AMPC steering outputs are much smoother after second number three. This phenomenon occurs because the model used by the AMPC is not accurate at the start of the simulation, however after approximately three seconds, the estimator reaches a steady state of the correct cornering stiffness values that affect the real car model to follow the desired reference signals from the reference ideal model. As a result, the AMPC makes incorrect predictions when optimizing steering output, resulting in oscillations in steering control. By using the estimated tire cornering stiffness values, the AMPC model updates the tire stiffness as the simulation progresses. In this way, the AMPC is able to perform better.

Both the front and rear tires were initially designed with cornering stiffnesses of 80 kN/rad and 100 kN/rad, respectively. For the first, second, and third steering inputs, the estimator determined the front tire stiffness to be 70 kN/rad, 68 kN/rad, and 69 kN/rad, respectively. Also, the rear tire stiffness should be set at 74 kN/rad, 78 kN/rad, and 77 kN/rad for the first, second, and third steering inputs, respectively. On the real car plant model, the final values for both front and rear estimated cornering stiffness were almost the same, demonstrating the performance of both AMPC controller and estimator.

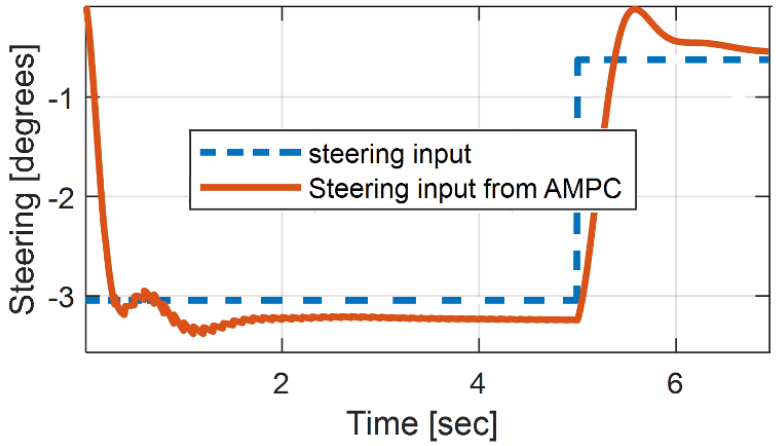

Figure (17). Steering input from user and AMPC

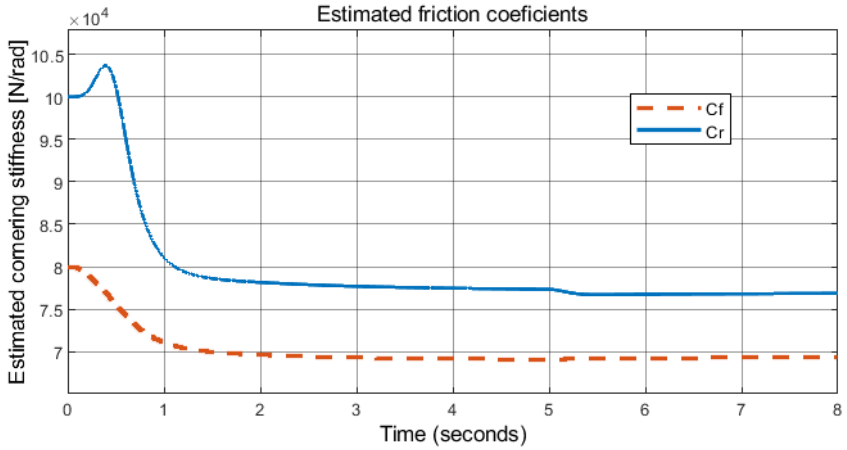

Figure (18). Estimated cornering stiffnesses for front and rear tires

7.1 Comparison among technologies

A comparison of the three used vehicles compared to the ideal vehicle is presented in Table 3 to demonstrate what technology should be used in vehicles to ensure stability and lateral comfort.

Table (3) Comparison between three vehicles corresponding to the ideal one.

	Uncontrolled real car	Controlled real car	Controlled real car with estimation
Steering angle	Same ideal (open loop)	Higher, with oscillations	Very closed, without oscillations
Yaw rate	Not following (unstable)	Closer (stable)	Almost same as ideal (stable)
Lateral acceleration	Not following ideal response (uncomfortable)	Closer to the ideal response (comfortable)	Almost same as ideal response (comfortable)

Estimated cornering stiffness	----	----	3 seconds to estimate correct values
Following ideal car's XY trajectory	Not following ideal path	closer to the ideal XY path	Almost ideal same XY path

According to the results of the previous table, the controlled vehicle with cornering stiffness estimator was the most stable and had the best lateral comfort with minimal oscillations of the steering angle from the controller. Additionally, it has at most the same XY trajectory path as the ideal vehicle for autonomous driving, so the results in this study indicate that controlled vehicles with estimators are the preferred technology.

7.2 Comparison among previous studies

Several papers in the field of vehicle dynamics and control have employed linear model predictive controllers (LMPCs) for improving the handling limits of yaw rate by actively steering the front of the vehicle (Li et al., 2020). Other papers used a long short-term memory network for cornering stiffness estimation, thereby providing significant information to a vehicle's direct yaw robust controller system in order to construct a lateral dynamic model. For enhancing performance and stability, other researchers have applied the Levenberg Marquardt approach (Pereira et al., 2021). In Table 4, the effectiveness of this research is compared with that of recent previous studies in terms of the development of an effective controller and estimation for stabilizing the lateral performance of ground vehicles.

Table (4) Comparison with previous studies

Comparisons		Approach / Study			Current Study
		Li et al. (2020)	**Lian et al. (2023)**	**Pereira et al. (2021)**	
Vehicles plant model Parameters	Number of tires	2 tires	4 tires	6 tires	4 tires
	Mass and yaw moment of inertia	1240 kg and 2031.4 $kg.m^2$	1159 kg and 617 $kg.m^2$	15770 kg and 63595 $kg.m^2$	1200 kg and 1500 $kg.m^2$
	Front and real cornering stiffness	52618 and 52185 N/rad	---- ----	400000, 300000 and 200000 N/rad	30000 and 40000 N/rad
	Longitudinal velocity	22.2 m/s	25 m/s	21.9 m/s	21 m/s
Control system	Type of controller	LAMPC	DYC robust controller	----	AMPC
	Speed of the control system implemented by rising time.	0.2 sec	0.7 sec	----	0.1 sec

	Inputs / Outputs of controller	/ yaw rate Front steering angle	yaw rate and sideslip angle/ front steering angle	----	yaw rate, lateral / Front acceleration steering angle
	Controlled yaw rate limits	4 rad/ sec	2.5 rad/sec	----	0.4 rad / sec
	Controlled lateral acceleration limits	----	----	----	4 m/sec^2
	Estimators used for tire stiffness	----	Long short-term memory network	Levenberg Marquardt	Least square recursive
Estimation	Time required to reach correct cornering stiffnesses	----	0.1 sec	8 sec	3 sec

8 CONCLUSIONS

The present study examined how AMPC controllers can be used to control the yaw rate and lateral acceleration of a nonlinear car's model using active front steering angle in conjunction with the prediction of cornering stiffness. The nonlinear plant model was linearized using an AMPC controller, and estimated cornering stiffnesses were updated into a linear ideal model based on a bicycle model. Models of real and ideal vehicles have been described and simulated using MATLAB software. The proposed yaw rate and lateral acceleration control system was tested in three separate ways in order to determine the optimal yaw rate, lateral acceleration, and XY trajectory. Based on the results of the study, AMPC performance is enhanced when used in conjunction with tire stiffness estimation. In addition, the estimator took approximately three seconds to reach the correct values for both front and rear tire stiffnesses. As a result, the controller was able to track the desired state responses even within a short period of time, about 0.1 seconds. A model of the proposed system could be developed using artificial intelligence (AI) for further research and development on the effects of the environment and the car as a result of input road maneuvers.

9 REFERENCES:

Wang, Y., Hu, J., Wang, F., Dong, H., Yan, Y., Ren, Y., Zhou, C., & Yin, G. (2022). Tire Road Friction Coefficient Estimation: Review and Research Perspectives. *Chinese Journal of Mechanical Engineering, 35*(2), 6.

Chen, G., Zhao, X., Gao, Z., & Hua, M. (2023). Dynamic drifting control for general path tracking of autonomous vehicles. *IEEE Transactions on Intelligent Vehicles, 8*(3), 2527-2537.

Yahagi, S., & Suzuki, M. (2023). Intelligent PI control based on the ultra-local model and Kalman filter for vehicle yaw-rate control. SICE Journal of Control, Measurement, and System Integration. *SICE Journal of Control, Measurement, and System Integration, 16*(1), 38-47.

Mietzner, J., Lampe, L., & Schober, R. (2009). Distributed transmit power allocation for multihop cognitive-radio systems. *IEEE Transactions on Wireless Communications, 8*(10), 5187-5201.

Blagojevic, V., & Ivanis, P. (2012). Ergodic capacity for TAS/MRC spectrum sharing cognitive radio. *IEEE Communications Letters, 16*(3), 321-323. https://arab-scholars.com/5bb1b1.

Yurtsever, E., Lambert, J., Carballo, A., & Takeda, K. (2020). A survey of autonomous driving: Common practices and emerging technologies. *IEEE access, 8,* 58443-58469.

Eskandarian, A., Wu, C., & Sun, C. (2019). Research advances and challenges of autonomous and connected ground vehicles. *IEEE Transactions on Intelligent Transportation Systems, 22*(2), 683-711.

Davis, S., & Boundy, R. (2021). *Transportation energy data book: Edition 39*. Oak Ridge National Lab.(ORNL), Oak Ridge, TN (United States).

Zhang, G., Wang, X., Li, L., & Zhao, X. (2023). Tire-Road Friction Estimation for Four-Wheel Independent Steering and Driving EVs Using Improved CKF and FNN. *IEEE Transactions on Transportation Electrification, 10*(1), 823-834.

Xu, N., Zhou, J., Barbosa Henrique Groenner, B., Askari, H., & Khajepour, A. (2023). A Soft Sensor for Estimating Tire Cornering Properties for Intelligent Tires. *IEEE Transactions on Systems, Man, and Cybernetics: Systems, 53*(10), 6056-6066.

Hajiloo, R., Abroshan, M., Khajepour, A., Kasaiezadeh, A., & Chen, S. (2020). Integrated steering and differential braking for emergency collision avoidance in autonomous vehicles. *IEEE Transactions on Intelligent Transportation Systems, 22*(5), 3167-3178.

Gao, H., Kan, Z., & Li, K. (2021). Robust lateral trajectory following control of unmanned vehicle based on model predictive control. *IEEE/ASME Transactions on Mechatronics, 27*(3), 1278-1287.

De Bernardis, M., Rini, G., Bottiglione, F., Hartavi, A., & Sorniotti, A. (2023). On nonlinear model predictive direct yaw moment control for trailer sway mitigation. *Vehicle system dynamics, 61(*2), 445-471.

Chen, Z., Xiong, R., Cai, X., Wang, Z., & Yang, R. (2023). Regenerative braking control strategy for distributed drive electric vehicles based on slope and mass co-estimation. *IEEE Transactions on Intelligent Transportation Systems, 24*(12), 14610-14619.

Shakouri, P., & Ordys, A. (2014). Nonlinear Model Predictive Control approach in design of Adaptive Cruise Control with automated switching to cruise control. *Control Engineering Practice, 26,* 160-177.

Nilsson, J., Silvlin, J., Brannstrom, M., Coelingh, E., & Fredriksson, J. (2016). If, When, and How to Perform Lane Change Maneuvers on Highways. *IEEE Intelligent Transportation Systems Magazine, 8*(4), 68-78.

Li, X., Sun, Z., Cao, D., He, Z., & Zhu, Q. (2015). Real-time trajectory planning for autonomous urban driving: Framework, algorithms, and verifications. *IEEE/ASME Transactions on mechatronics, 21*(2), 740-753.

Wang, N., Lv, S., Er, M., & Chen, W. (2016). Fast and accurate trajectory tracking control of an autonomous surface vehicle with unmodeled dynamics and disturbances. *IEEE Transactions on Intelligent Vehicles, 1*(3), 230-243.

Daily, R., & Bevly, D. (2004). The use of GPS for vehicle stability control systems. *IEEE transactions on industrial electronics, 51(*2), 270-277.

Nishio, A., Tozu, K., Yamaguchi, H., Asano, K., & Amano, Y. (2001). Development of vehicle stability control system based on vehicle sideslip angle estimation. *SAE transactions, 110*(6), 115-122.

Zhang, B., Du, H., Lam, J., Zhang, N., & Li, W. (2016). A Novel Observer Design for Simultaneous Estimation of Vehicle Steering Angle and Sideslip Angle. *IEEE Transactions on Industrial Electronics, 36*(7), 4357-4366.

Pacejka, H. (2005*). Tire and vehicle dynamics* (2nd ed.). Elsevier.

Hayward, R., Marchick, A., & Powell, J. (1999). Two antenna GPS attitude and integer ambiguity resolution for aircraft applications. Pro*ceedings of the 1999 National Technical Meeting of The Institute of Navigation,* 155-164.

Cohen, C., Parkinson, B., & McNally, B. (1994). Flight tests of attitude determination using GPS compared against an inertial navigation unit. *Navigation, 41*(1), 83-97.

Acosta, M., Kanarachos, S., & Blundell, M. (2019). Virtual tyre force sensors: An overview of tyre model-based and tyre model-less state estimation techniques. Proceedings of the Institution of Mechanical Engineers, Part D: *Journal of Automobile Engineering, 232*(14), 1883-1930.

Li, S., Wang, G., Zhang, B., Yu, Z., & Cui, G. (2020). Vehicle yaw stability control at the handling limits based on model predictive control. *International Journal of Automotive Technology*, *21,* 361-370.

Lian, Y., Feng, W., Liu, S., & Nie, Z. (2023). A Road Adhesion Coefficient-Tire Cornering Stiffness Normalization Method Combining a Fractional-Order Multi-Variable Grey Model with a LSTM Network and Vehicle Direct Yaw-Moment Robust Control. *Frontiers in Neurorobotics, 17,* 1229808.

Pereira, C., da Costa Neto, R., & Loiola, B. (2021). Cornering stiffness estimation using Levenberg–Marquardt approach. *Inverse Problems in Science and Engineering, 29*(12), 2207-2238.